Hindawi Publishing Corporation
EURASIP Journal on Advances in Signal Processing
Volume 2007, Article ID 49482, 8 pages
doi:10.1155/2007/49482

*Research Article*

# Statistical Segmentation of Regions of Interest on a Mammographic Image

**Mouloud Adel,[1] Monique Rasigni,[1] Salah Bourennane,[1] and Valerie Juhan[2]**

[1] *Institut Fresnel, UMR-CNRS 6133, Equipe GSM, Domaine Universitaire de Saint-Jérôme, Avenue Escadrille Normandie Niemen, 13397 Marseille Cedex 20, France*
[2] *Service de Radiologie, Hôpital de la Timone, 27, Boulevard Jean Moulin, 13385 Marseille Cedex 5, France*

Received 16 November 2006; Revised 11 April 2007; Accepted 13 May 2007

Recommended by Jiri Jan

This paper deals with segmentation of breast anatomical regions, pectoral muscle, fatty and fibroglandular regions, using a Bayesian approach. This work is a part of a computer aided diagnosis project aiming at evaluating breast cancer risk and its association with characteristics (density, texture, etc.) of regions of interest on digitized mammograms. Novelty in this paper consists in applying and adapting Markov random field for detecting breast anatomical regions on digitized mammograms whereas most of previous works were focused on masses and microcalcifications. The developed method was tested on 50 digitized mammograms of the mini-MIAS database. Computer segmentation is compared to manual one made by a radiologist. A good agreement is obtained on 68% of the mini-MIAS mammographic image database used in this study. Given obtained segmentation results, the proposed method could be considered as a satisfying first approach for segmenting regions of interest in a breast.



## 1. INTRODUCTION

Breast cancer is the leading cause of death among all cancers for middle-aged women. Currently it affects one woman out of eight and an increase of this rate in the nearest future is expected. For the last 40 years, extensive means have been devoted to tackling this disease but without the expected success. Efforts are now focused on early detection and prevention. It is now known that screening programs reduce the mortality rate of about 30% for middle-aged women. At present, mammography is the current standard for early breast cancer detection.

Mammographic images are difficult to analyse due to wide variation of anatomical patterns of each breast. One important task for radiologists when reading mammograms consists in evaluating the proportion of fatty and fibroglandular tissue with respect to the whole breast. Mammographic density is known to be an important indicator of breast cancer risk. There are four metrics which are used in practice to relate the mammographic parenchymal patterns and the risk of breast cancer, namely: Wolfe's four parenchymal patterns [1], Boyd's six class categories [2], BI-RADS [3], and Tabár's five patterns [4]. The comparative study of these four approaches on MIAS database [5] in particular has been reported in [6]. In first studies devoted to computer aided diagnosis and early detection of breast cancer using image processing techniques, analysis was performed on the whole image without taking into account different density, texture and anatomic region levels, that radiologists use in their interpretation [7]. Other methods have been proposed for anatomic region segmentation on digitized mammograms [8–12]. Aylward et al. [8] divided a mammographic image into five regions and then used geometric and statistical techniques. Ferrari et al. [9] segmented the peripheral breast tissue with an automatic thresholding method based on Lloyd-Max quantification. Matsubara et al. [10] segmented the fibroglandular tissue by means of horizontal and vertical histogram variance computation followed by a local discriminant analysis. Zhou et al. [11] used a three-step segmentation method to locate the fibroglandular edges whereas Ferrari et al. [12] segmented the fibroglandular disc with a statistical method based on a Gaussian mixture modelling.

Other segmentation methods have been developed in the literature but did not focus on anatomical region segmentation. Specific problems such as peripheral breast tissue correction [13, 14], nipple automatic localization [15], breast density quantification [16], and its association with the risk of breast cancer [17–22] have been also investigated.

However, most of classification results in comparison with expert assessment tend to be low. Masek et al. [23] used average histograms of each original image density class as a feature and reported an agreement of 62.42% whereas Zwiggelaar et al. [24] and Muhimmah and Zwiggelaar [25] obtain an agreement of 71.50% and 77.57% when using statistical grey-level histogram modeling and classification based on multiresolution histogram information, respectively.

This paper deals with Bayesian segmentation of breast anatomical regions, namely: the pectoral muscle, the fibroglandular and fatty regions, on digitized mammograms. Novelty in this paper is in applying and adapting a Markov random field for detecting region of different tissues on mammographic digitized images whereas most of previous works were focused on abnormalities (masses and microcalcifications). One of the objectives of this study is to provide radiologists with computer aided classification tool for discriminating anatomical breast regions on a digitized mammograms and then for determining more accurate proportion of fatty and fibroglandular tissue with respect to whole breast. Moreover, this study is a part of computer aided diagnosis project aiming at studying risk of developing a breast cancer and its association with the mammographic parenchymal patterns.

After a brief introduction to Markov random fields (MRF) and Bayesian segmentation in Section 2, the method is developed and applied on digitized mammograms in Section 3. Section 4 shows obtained results. Finally, Section 5 gives conclusions of the work.

## 2. MARKOV RANDOM FIELDS AND BAYESIAN SEGMENTATION

### 2.1. Image model and Markov random fields

The main regions of interest in a mammogram are shown in Figure 1. They are the pectoral muscle, the fibroglandular and fatty tissues. Background outside the breast is not considered as a region of interest but it will be taken into account for the segmentation process.

In this study, a statistical segmentation approach is adopted. It consists in considering the observed mammographic image as a realization $y$ of a random field $Y$. Segmenting regions of interest amounts to estimating the label field $X$ (segmented version where each pixel is assigned a label representing one of the regions described above).

Fields $X$ and $Y$ are defined on a rectangular lattice $S$ of $N$ pixels. To each spatial location $(i, j)$ or each site $s$ of $S$ is associated a random variable $X_{(i,j)}$ or $X_s$. Random variables $X_s$ take their values in a set $E = \{0, 1, 2, \ldots, M\}$, where $M$ is the number of classes. The set of all possible realizations $x$ of $X$ is denoted by $\Omega_X$.

By another way a neighborhood system $V_s$ of a pixel $s \in S$ is defined as follows:

$$V_s = \{t \in S\} \quad \text{such that } \{s \notin V_s,\ t \in V_s \Longrightarrow s \in V_t\},$$
$$V = \{V_s,\ s \in S\}. \tag{1}$$

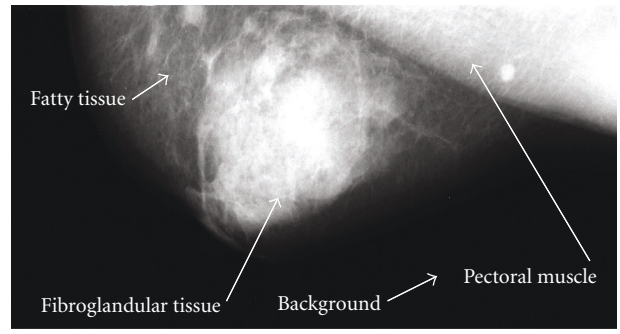


Figure 1: Digitized mammogram with its regions of interest.

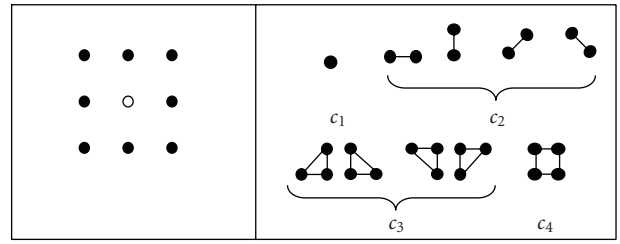


Figure 2: Cliques induced by the eight-point nearest-neighbour system.

Given a neighborhood system $V_s$, a clique $c \subset S$ is either a single site (singleton), or a subset of sites in which each pair of distinct sites is the neighbor of each other. Cliques with only one pixel are denoted by $c_1$, those with 2 pixels by $c_2$ and so on.

For instance Figure 2 shows cliques in an eight-nearest neighborhood system.

Then $X$ is a Markov random field (MRF) relatively to a neighbourhood system $V$ if and only if

$$\begin{aligned} &\text{(a) } \forall x \in \Omega_X, \quad P(X = x) > 0 \\ &\text{(b) } \forall s \in S, \quad P(X_s = x_s | X_t = x_t,\ t \in S - \{s\}) \\ &\qquad\qquad = P(X_s = x_s | X_s = x_t,\ t \in V_s), \end{aligned} \tag{2}$$

where $P(A/B)$ stands for the conditional probability of the event $A$ given the event $B$. Property (b) shows that probability associated with random variable $X_s$ depends only on neighbours of site $s$. According to Hammersley-Clifford theorem [26], an MRF $X$ relatively to a neighborhood system $V$ can equivalently be characterized by a Gibbs distribution, that is, the probability $P(X = x)$ can be expressed in the form

$$P(X = x) = \frac{1}{Z} \exp\left( - \sum_{c \in C} U_c(x) \right),$$
$$Z = \sum_{x \in \Omega_X} \exp\left( - \sum_{c \in C} U_c(x) \right), \tag{3}$$

where $U_c(\mathrm{x})$, known as clique potential function, denotes statistical dependence between pixels within a clique and thus depends only on the pixels that belong to this clique $c$. $C$ is the set of all possible cliques $c$ on $S$ for the neighborhood

system $V$ under consideration. $\sum_{c\in C} U_c(x)$ is an energy function. At last $Z$ is a normalizing constant called the partition function.

### 2.2. Bayesian segmentation

Image statistical segmentation schemes are generally based on optimization of some criterion. In our approach on mammoghraphic images, the maximum *a* posteriori (MAP) estimate of the label field $X$ given the observed image $y$ is used.

According to Bayes rule, we have

$$P(X = x|Y = y) = \frac{P(Y = y|X = x)P(X = x)}{P(Y = y)}, \quad (4)$$

where $P(X = x)$ is the prior probability given by (3) and $P(Y = y)$ is a constant when $y$ is a given observed image. The MAP estimate is found by maximizing $P(Y = y|X = x)P(X = x)$.

Probability $P(Y = y|X = x)$ can be computed on the following assumptions:

(a) random variables $Y_s$, $s \in S$, are conditionally independent given the label field $X$. In this case:

$$P(Y = y|X = x) = \prod_{s\in S} P(Y_s = y_s|X_s = x_s) \quad (5)$$

(b) conditional probabilities $P(Y_s = y_s|X_s = x_s)$ satisfy a given model, for instance a Gaussian one.

Then it ensues from (3) and (5) that the *a posteriori* probability given by (4) may be expressed as

$$P(X = x|Y = y) \propto \exp\left(\sum_{s\in S} \mathrm{Ln}\left(P(Y_s = y_s|X_s = x_s)\right) - \sum_{c\in C} U_c(x)\right). \quad (6)$$

Equation (6) may be also written in the form

$$P(X = x|Y = y) \propto \exp\left(-U\Big(X = x|Y = y\Big)\right) \quad (7)$$

$$\text{with } U(X = x|Y = y) = -\sum_{s\in S} \mathrm{Ln}\left(P(Y_s = y_s|X_s = x_s)\right) + \sum_{c\in C} U_c(x). \quad (8)$$

Equation (7) shows that the label field $X$ given observed image y is characterized by a Gibbs distribution and so that it is a Markov random field too. The MAP estimate is equivalently obtained by minimizing a posteriori energy $U(X = x|Y = y)$ (8).

## 3. SEGMENTATION OF MAMMOGRAPHIC IMAGES

### 3.1. Statistical model used

The above method is applied to digitized mammograms with the following assumptions:

(a) regions to be segmented and classes are denoted by region $R_i$ and class $i$, respectively;

(b) the conditional probability density function of random variable $Y_s$, $s \in S$ $P(Y_s = y_s|X_s = x_s)$, is assumed to be Gaussian, that is,

$$P(Y_s = y_s|X_s = x_s) = \frac{1}{\sqrt{2\pi}\sigma_i} \exp\left(-\frac{(y_s - \mu_i)^2}{2\sigma_i^2}\right), \quad (9)$$

where $\mu_i$ and $\sigma_i^2$ are the mean and the variance of class $i$ to which $x_s$ is associated with. On the other hand, a relatively simple type of discrete-valued MRF called multilevel logistic (MLL) may be used for modeling region formation in image segmentation [27]. In our approach, the eight-nearest neighbour system (Figure 2) is used, and because, cliques containing more than 2 pixels cause too much computational complexity, the only nonzero potentials of the MLL are assumed to be those corresponding to two-pixel cliques. The potential function $U_c(x)$ of a two-pixel clique $c$ associated with a site $s$ is then defined by [28]

$$U_c(x) = \begin{cases} +\beta_c & \text{if } x_t = x_s\, s, t \in c, \\ -\beta_c & \text{otherwise,} \end{cases} \quad (10)$$

where the parameter $\beta_c$ is the same for every two-pixel clique, that is to say $\beta_c = \beta$. The value of $\beta$ influences the sizes and shapes of the resulting regions: as $\beta$ increases larger clusters are favored [29].

So the *a posteriori* energy $U$ (8) becomes

$$U(X = x|Y = y) = \sum_{s\in S}\left(\left(\frac{(y_s - \mu_{x_s})^2}{2\sigma_{x_s}^2}\right) + \mathrm{Ln}\left(\sqrt{2\pi}\sigma_{x_s}\right)\right) + \sum_{c\in C_2} U_c(x), \quad (11)$$

where $\mu_{x_s}$ and $\sigma_{x_s}^2$ are the mean and the variance of the class to which $x_s$ is associated with and $C_2$ is the set of all two-pixel cliques.

### 3.2. Initialization and parameters estimation

Mammographic image segmentation scheme is obtained from three main steps:

(a) initialization of label field $X$ with a choice of class number $M$

(b) estimate of model parameters and label field simulation using optimization methods for minimizing the *a posteriori* energy $U$ (11);

(c) stopping condition.

The two last stages (b) and (c) are iterative processes.

In this work, three initializations are tested as follows.

(i) Equal probability quantizing [30] which splits the grey level range of image $y$ into several classes using the probability cumulative function of the image according to an iterative process. This initialization is denoted INIT A.

(ii) Uniform quantizing of the grey-level range of image $y$. This initialization is denoted by INIT B.

(iii) An identical number of pixels per class. This initialization is denoted by INIT C.

For each initialization, the number of classes was limited to five.

Computation of the *a posteriori* $U$ energy (11) needs mean and variance estimates for each class. These parameters are supposed unknown but are fixed. They were estimated from the empirical Bayesian method according to the following formulas:

$$\begin{aligned} \hat{\mu}_i^{(k)} &= \frac{1}{N_i^{(k)}} \sum_{s \in R_i^{(k)}} y_s, \\ \left(\hat{\sigma}_i^2\right)^{(k)} &= \frac{1}{N_i^{(k)}} \sum_{s \in R_i^{(k)}} \left(y_s - \hat{\mu}_i^{(k)}\right)^2, \end{aligned} \tag{12}$$

where $R_i$ stands for region whose pixels belong to class $i$, $N_i$ is the number of pixels in $R_i$ and $k$ is used to specify the current iteration.

Among several algorithms [31] used for $U$ minimization, two algorithms are proposed to find a reasonably good labeling: simulated annealing (SA) [32] because it is probabely one of the best known, and the Iterated conditional modes (ICM) [33] which is a fast deterministic version of SA and provides good segmentation if a good initial segmentation is available.

Simulated annealing is an algorithm dedicated to searching the optimal configuration of a Gibbs field. For each site $s$, a label $\lambda$ is chosen at random in the label set $E$ and the following energy variation is evaluated:

$$\Delta U_s = U_s\left(X_s = \lambda \mid V_s^{(k)}\right) - U_s\left(X_s = x_s^{(k)} \mid V_s^{(k)}\right), \tag{13}$$

where $U_s$ is computed from (11) by considering only the site $s$ and its neighborhood $V_s$, $x_s^{(k)}$ and $V_s^{(k)}$ are the label and neighborhood of site $s$ at iteration $k$, respectively. The $\beta$ value, $\beta = 50$ used for clique potential $U_c(x)$ evaluation was chosen as the one yielding the best visual segmentation on several preliminary tests. Label of site $s$ is then updated with label $\lambda$ if $\Delta U_s \geq 0$. Otherwise ($\Delta U_s < 0$), label of site $s$ takes the $\lambda$ value or keeps its previous value according to probabilities $p$ and $1 - p$ respectively ($p = \exp(-\Delta U_s)$).

ICM is also an iterative algorithm which aims at minimizing $U$ ((11)). For each site $s$ this method computes the local conditional probabilities

$$P\left(X_s = \lambda \mid X_r = x_r^{(k)},\ r \in V_s\right) \tag{14}$$

for every label $\lambda$ of label set $E$. Label of site $s$ is then updated with the value which maximizes these probabilities, that is, at iteration $k + 1$:

$$x_s^{(k+1)} = \operatorname*{Arg\,max}_{\lambda} P\left(X_s = \lambda \mid X_r = x_r^{(k)},\ r \in V_s\right). \tag{15}$$

This algorithm is faster than the SA but needs a good initialization for converging.

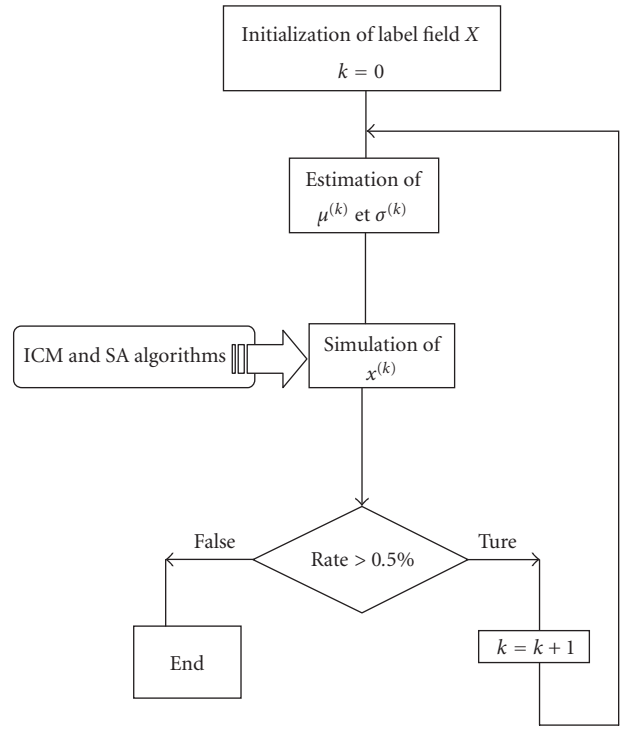


Figure 3: Mammographic image segmentation scheme.

Last stage in the segmentation process concerns the stopping condition. This condition is based on the rate of pixels changing their label between two iterations, that is

$$\begin{aligned} \text{rate} &= \frac{\sum_{s \in S}\left(1 - \delta\left(x_s^{(k+1)}, x_s^{(k)}\right)\right)}{N}, \\ \text{with } \delta\left(x_s^{(k+1)}, x_s^{(k)}\right) &= \begin{cases} 1 & \text{if } x_s^{(k+1)} = x_s^{(k)}, \\ 0 & \text{else,} \end{cases} \end{aligned} \tag{16}$$

where $k$ stands for the current iteration, $N$ is the number of pixels in image $y$. When this rate is less than a given threshold, the segmentation process stops. For this study we felt a thresholding of 0.5% was small enough. The segmentation scheme is summarized in Figure 3.

## 4. RESULTS AND DISCUSSION

Fifty digitized mammograms of the mini-Mammographic Image Analysis Society (MIAS) database with different anatomical patterns were chosen with the help of radiologists, for evaluating the proposed method. Images of mini-MIAS are those of MIAS database [5] (mammograms digitized at 50 $\mu$m/pixel) reduced to 200 $\mu$m/pixel and clipped/padded so that every image is $1024 \times 1024$ pixels. This database is given with a classification into three classes: fatty (F), glandular (G), and dense (D) breasts. Only normal cases were chosen for this study and the proportions within each class were 16, 18, and 16 for fatty, glandular, and dense, respectively. Radiologists were asked to define manually the fibroglandular and the fatty regions as well as the pectoral

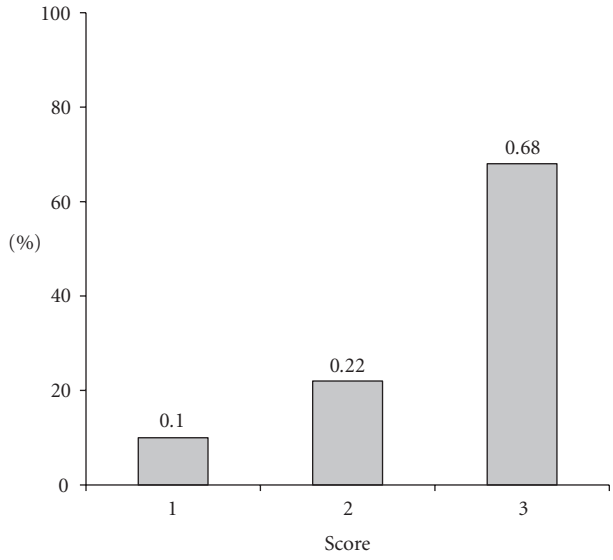


Figure 4: Rating of segmentation results.

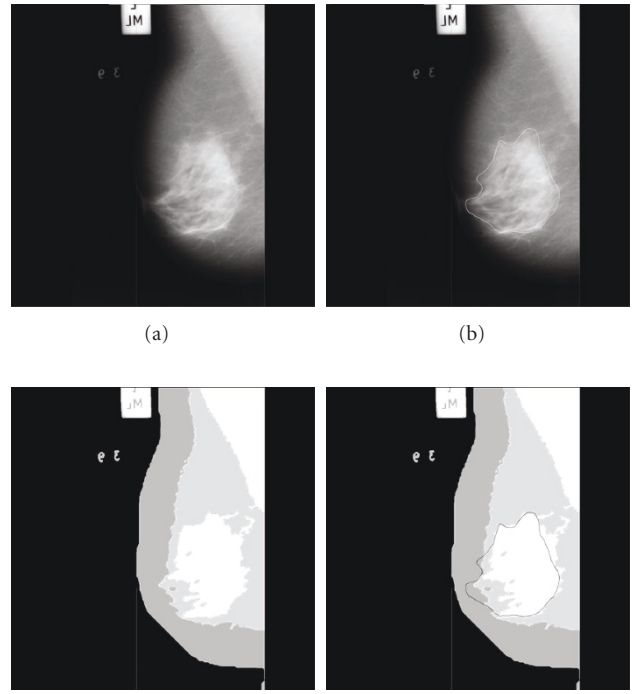

(a) (b) (c) (d)

Figure 5: Segmentation results: (a) original mammogram mdb041; (b) radiologist's manual segmentation; (c) obtained segmentation with initialization INIT A and ICM algorithm (10 iterations); (d) obtained segmentation compared to radiologist's manual segmentation ($\rho = 0.77$).

muscle on each image. This work was done by means of a computer monitor with IDL/ENVI software.

Evaluation of segmentation results concerns only fibroglandular tissue. Indeed the ratio of fibroglandular region in comparison with the whole breast region is of importance for radiologists when interpreting mammograms. In particular, it has been noticed clinically that majority of breast cancers were associated with glandular rather than fatty tissues [34].

For each mammographic image, a quality parameter $\rho$ and a protocol [12] were introduced for quantifying segmentation results. Parameter $\rho$ was defined as follows:

$$\rho = \frac{|A_{\text{seg}} \cap A_{\text{manu}}|}{|A_{\text{seg}} \cup A_{\text{manu}}|}, \tag{17}$$

where $A_{\text{seg}}$ is the set of pixels of the fibroglandular region obtained by computer segmentation and $A_{\text{manu}}$ is the set of pixels of the same region by manual segmentation. $|A|$ is the number of elements of set $A$.

A score was then associated with each result according to the description given in Table 1.

Actually, final results of iterative segmentation algorithms used in this work depend mainly on the initialization step. In theory, simulated annealing (SA) makes it possible to reach a global minimum whatever the initialization conditions are, but this goal is not always obtained and the SA converges often to a local minimum. In the case of ICM, initialization must be close to final solution to assure a good segmentation.

Except for some few cases, Init A (equal probability quantizing) is the initialization method which gave the best segmentation results for ICM and SA. Segmentations obtained by both optimization methods (SA and ICM) were similar with nevertheless higher number of iterations for simulated annealing (SA). Results ratings related to protocol

Table 1: Ranking options for evaluation of segmentation results.

| | |
|---|---|
| Score = 3 if $60\% \le \rho \le 100\%$ | Good segmentation |
| Score = 2 if $20\% \le \rho \le 60\%$ | Average segmentation |
| Score = 1 if $\rho \le 20\%$ | Failed segmentation |

given in Table 1 are shown in Figure 4. This table summarizes the best results obtained when combining Initialization methods (INIT A, INIT B,s and INIT C) and optimization algorithms (SA and ICM).

Approximately 68% of the cases (34 mammograms) were rated as good segmentation (score 3) (agreement between manual and computer segmentations higher than 60%). These mammograms are those associated with D (dense) and G (glandular) classes where the fibroglandular tissue constituted a compact region and, in most of the cases separated from the pectoral muscle (Figure 5).

For medium scores (score 2) (agreement between manual and computer segmentations is between 20% and 60%), the segmentation method underestimated the fibroglandular regions. On these mammograms fibroglandular regions were surrounded by fibrous structure and their edges were not very sharp. Results obtained on such mammograms are shown in Figure 6. Among the remaining cases (5 mammograms) lowest scores (score 1) (agreement between manual and computer segmentation lower than 20%) were obtained for breasts with a very small fibroglandular region, which

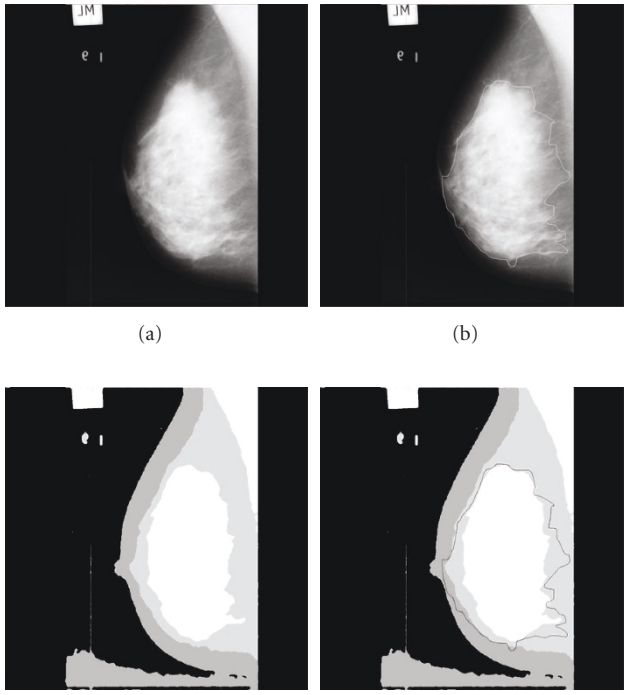

(a) (b)

(c) (d)

Figure 6: Segmentation results: (a) original mammogram mdb003; (b) radiologist's manual segmentation; (c) obtained segmentation with initialization INIT A and SA algorithm (80 iterations); (d) obtained segmentation compared to radiologist's manual segmentation ($\rho = 0.58$).

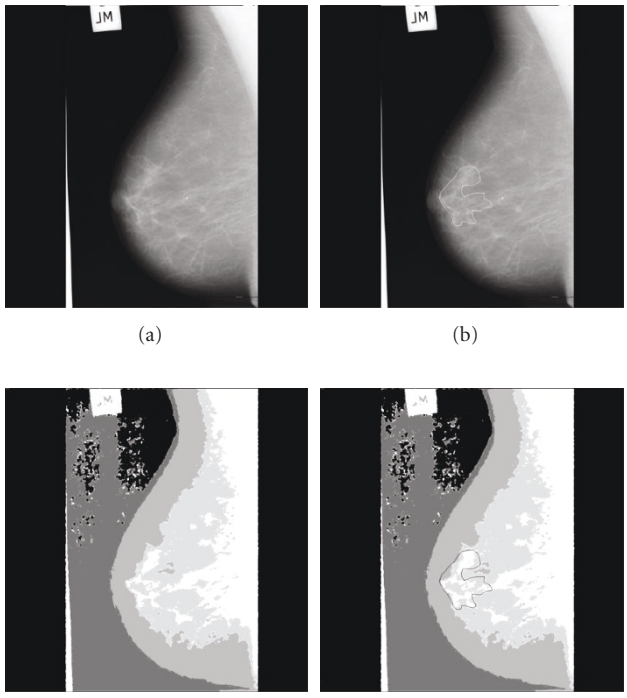

(a) (b)

(c) (d)

Figure 7: Segmentation results: (a) original mammogram mdb009; (b) radiologist's manual segmentation; (c) obtained segmentation with initialization INIT A and SA algorithm (78 iterations); (d) obtained segmentation compared to radiologist's manual segmentation ($\rho = 0.185$).

could be interpreted as fatty breasts by radiologists. Moreover, fatty tissue was observed inside the fibroglandular region of these mammograms. For these cases the segmentation method underestimated the fibroglandular regions (Figure 7).

## 5. CONCLUSION

In this paper, a Bayesian segmentation approach with a Markov random field model is presented and applied to regions of interest on digitized mammographic images. Bayesian method was used for estimating model parameters as well as the MAP as optimization criterion. The obtained results are promising and lead us to consider this method as a satisfying approach for segmenting breast regions of interest. An evaluation of this method on a large image base is needed now. Likewise characterization of the segmented regions by means of some parameters in order to correlate them with false negatives breast cancer will constitute a future step of this work.

## REFERENCES

[1] J. N. Wolfe, "Risk for breast cancer development determined by mammographic parenchymal pattern," *Cancer*, vol. 37, no. 5, pp. 2486–2492, 1976.

[2] N. F. Boyd, J. W. Byng, R. A. Jong, et al., "Quantitative classification of mammographic densities and breast cancer risk: results from the Canadian National Breast Screening study," *Journal of the National Cancer Institute*, vol. 87, no. 9, pp. 670–675, 1995.

[3] ACR, *Breast Imaging Reporting and Data System (BI-RADS)*, American College of Radiology, Reston, Va, USA, 2nd edition, 1995.

[4] L. Tabár, T. Tot, and P. B. Dean, *Breast Cancer: The Art and Science of Early Detection with Mammography*, Georg Thieme, Stuttgart, Germany, 2005.

[5] J. Suckling, J. Parker, D. R. Dance, et al., "The mammographic image analysis society digital mammogram database," in *Proceedings of the 2nd International Workshop on Digital Mammography*, vol. 1069 of *Exerpta Medica, International Congress Series*, pp. 375–378, York, England, July 1994.

[6] I. Muhimmah, A. Oliver, E. R. E. Denton, J. Pont, E. Pérez, and R. Zwiggelaar, "Comparison between Wolfe, Boyd, BI-RADS and Tabár based mammographic risk assessment," in *Proceedings of the 8th International Workshop on Digital Mammography (IWDM '06)*, vol. 4046 of *Lecture Notes in Computer Science*, pp. 407–415, Manchester, UK, June 2006.

[7] R. M. Rangayyan, *Biomedical Image Analysis*, CRC Press, Boca Raton, Fla, USA, 2005.

[8] S. R. Aylward, B. M. Hemminger, and E. D. Pisano, "Mixture modeling for digital mammogram display and analysis," in *Proceedings of the 4th International Workshop on Digital Mammography (IWDM '98)*, pp. 305–312, Nijmegen, The Netherlands, June 1998.

[9] R. J. Ferrari, R. M. Ragayyan, J. E. L. Desautels, and A. F. Frere, "Segmentation of mammograms: identification of the skin-air

boundary, pectoral muscle, and fibro-glandular disc," in *Proceedings of the 5th International Workshop on Digital Mammography (IWDM '00)*, pp. 573–579, Toronto, Canada, June 2000.

[10] T. Matsubara, D. Yamazaki, H. Hara, T. Iwase, and T. Endo, "An automated classification method for mammograms based on evaluation of fibroglandular breast tissue density," in *Proceedings of the 5th International Workshop on Digital Mammography (IWDM '00)*, pp. 737–741, Toronto, Canada, June 2000.

[11] C. Zhou, H. P. Chan, N. Petrick, et al., "Computerized image analysis: estimation of breast density on mammograms," *Medical Physics*, vol. 28, no. 6, pp. 1056–1069, 2001.

[12] R. J. Ferrari, R. M. Rangayyan, R. A. Borges, and A. F. Frère, "Segmentation of the fibro-glandular disc in mammograms using Gaussian mixture modelling," *Medical and Biological Engineering and Computing*, vol. 42, no. 3, pp. 378–387, 2004.

[13] U. Bick, M. L. Giger, R. A. Schmidt, R. M. Nishikawa, and K. Doi, "Density correction of peripheral breast tissue on digital mammograms," *Radio Graphics*, vol. 16, no. 6, pp. 1403–1411, 1996.

[14] J. W. Byng, J. P. Critten, and M. J. Yaffe, "Thickness-equalization processing for mammographic images," *Radiology*, vol. 203, no. 2, pp. 564–568, 1997.

[15] R. Chandrasekhar and Y. Attikiouzel, "A simple method for automatically locating the nipple on mammograms," *IEEE Transactions on Medical Imaging*, vol. 16, no. 5, pp. 483–494, 1997.

[16] P. K. Saha, J. K. Udupa, E. F. Conant, D. P. Chakraborty, and D. Sullivan, "Breast tissue density quantification via digitized mammograms," *IEEE Transactions on Medical Imaging*, vol. 20, no. 8, pp. 792–803, 2001.

[17] J. W. Byng, N. F. Boydt, E. Fishell, R. A. Jong, and M. J. Yaffe, "The quantitative analysis of mammographic densities," *Physics in Medicine and Biology*, vol. 39, no. 10, pp. 1629–1638, 1994.

[18] J. W. Byng, N. F. Boyd, E. Fishell, R. A. Jong, and M. J. Yaffe, "Automated analysis of mammographic densities," *Physics in Medicine and Biology*, vol. 41, no. 5, pp. 909–923, 1996.

[19] P. G. Tahoces, J. Correa, M. Souto, L. Gomez, and J. J. Vidal, "Computer-assisted diagnosis: the classification of mammographic breast parenchymal patterns," *Physics in Medicine and Biology*, vol. 40, no. 1, pp. 103–117, 1995.

[20] N. Karssemeijer, "Automated classification of parenchymal patterns in mammograms," *Physics in Medicine and Biology*, vol. 43, no. 2, pp. 365–378, 1998.

[21] Z. Huo, M. L. Giger, W. Zhong, and O. I. Olopade, "Analysis of relative contributions of mammographic features and age to breast cancer risk prediction," in *Proceedings of the 5th International Workshop on Digital Mammography (IWDM '00)*, pp. 732–736, Toronto, Canada, June 2000.

[22] R. Sivaramakrishna, N. A. Obuchowski, W. A. Chilcote, and K. A. Powell, "Automatic segmentation of mammographic density," *Academic Radiology*, vol. 8, no. 3, pp. 250–256, 2001.

[23] M. Masek, S. M. Kwok, C. J. S. deSilva, and Y. Attikiouzel, "Classification of mammographic density using histogram distance measures," in *Proceedings of the World Congress on Medical Physics and Biomedical Engineering*, p. 1, Sydney, Australia, August 2003, CD-ROM.

[24] R. Zwiggelaar, I. Muhimmah, and E. R. E. Denton, "Mammographic density classification based on statistical grey-level histogram modeling," in *Proceedings of the Medical Image Understanding and Analysis (MIUA '05)*, pp. 183–186, Bristol, UK, July 2005.

[25] I. Muhimmah and R. Zwiggelaar, "Mammographic density classification using multiresolution histogram information," in *Proceedings of the International Special Topic Conference on Information Technology in Biomedicine (ITAB '06)*, Ioannina, Greece, October 2006.

[26] J. Besag, "Spatial interaction and the statistical analysis of lattice systems," *Journal of the Royal Statistical Society. Series B*, vol. 36, no. 2, pp. 192–236, 1974.

[27] R. C. Dubes, A. K. Jain, S. G. Nadabar, and C. C. Chen, "MRF model-based algorithms for image segmentation," in *Proceedings of International Conference on Computer Applications in Shipbuilding (ICCAS '90)*, pp. 808–814, 1990.

[28] S. Lakshmanan and H. Derin, "Simultaneous parameter estimation and segmentation of Gibbs random fields using simulated annealing," *IEEE Transactions on Pattern Analysis and Machine Intelligence*, vol. 11, no. 8, pp. 799–813, 1989.

[29] N. Karssemeijer, "Stochastic model for automated detection of calcifications in digital mammograms," *Image and Vision Computing*, vol. 10, no. 6, pp. 369–375, 1992.

[30] R. M. Haralick, K. Shanmugam, and I. Dinstein, "Textural features for image classification," *IEEE Transactions on Systems, Man and Cybernetics*, vol. 3, no. 6, pp. 610–621, 1973.

[31] M. Berthod, Z. Kato, S. Yu, and J. Zerubia, "Bayesian image classification using Markov random fields," *Image and Vision Computing*, vol. 14, no. 4, pp. 285–295, 1996.

[32] S. Geman and D. Geman, "Stochastic relaxation. Gibbs distributions and the Bayesian restoration of images," *IEEE Transactions on Pattern Analysis and Machine Intelligence*, vol. 6, no. 6, pp. 721–741, 1984.

[33] J. Besag, "On the statistical analysis of dirty pictures," *Journal of the Royal Statistical Society. Series B*, vol. 48, no. 3, pp. 259–302, 1986.

[34] S. Caulkin, S. Astley, J. Asquith, and C. Boggis, "Sites of occurrence of malignancies in mammograms," in *Proceedings of the 4th International Workshop on Digital Mammography (IWDM '98)*, pp. 279–282, Nijmegen, The Netherlands, June 1998.

**Mouloud Adel** received his Engineering degree in electrical engineering in 1990 from the Ecole Nationale Supérieure d'Electricité et de Mécanique (ENSEM) of Nancy, France, and his Ph.D. degree from the Institut National Polytechnique de Lorraine (INPL) of Nancy, in 1994. He is Professor Assistant at the Institut Universitaire de Technologie de Marseille and his research interests include image and signal processing for industrial inspection and computer aided detection and diagnosis for medical applications.

**Monique Rasigni** received the Doctorate degree in physics from the University of Marseille, France, in 1977. Since 2006, she is an Emeritus Professor at the University of Aix-Marseille III. After numerous works mainly devoted to surface roughness, order, disorder, and percolation through graph theory, her research interest is oriented, for some years now, towards medical image processing (mammograms and retinal angiograms).

**Salah Bourennane** received his Ph.D. degree from Institut National Polytechnique de Grenoble, France, in 1990 in signal processing. Currently, he is a full Professor at the Ecole Centrale de Marseille, France. His research interests are in statistical signal processing, array processing, image processing, tensor signal processing, and performances analysis.

**Valerie Juhan** is a Radiologist since 1997. She leads the Department of Women's Imaging at the University Hospital la Timone in Marseille, France. The main activity of this department is screening, diagnosis, and follow up of breast cancer, using mammography, breast US, and percutaneous imaging-guided core biopsy. Valerie Juhan's research interests include new technologies of breast exploration.